PCCP

Accepted Manuscript

ROYAL SOCIETY OF CHEMISTRY

www.rsc.org/pccp

Journal Name

RSCPublishing

ARTICLE

Ligand-size dependent water proton relaxivities in ultrasmall gadolinium oxide nanoparticles and in vivo T_1 MR images in a 1.5 T MR field

Cite this: DOI: 10.1039/x0xx00000x

Received 00th January 2012,
Accepted 00th January 2012

DOI: 10.1039/x0xx00000x

www.rsc.org/

Cho Rong Kim,[a] Jong Su Baeck,[b] Yongmin Chang,*[b,c] Ji Eun Bae,[c] Kwon Seok Chae,[c,d] and Gang Ho Lee*[a,c]

The dependence of longitudinal (r_1) and transverse (r_2) water proton relaxivities of ultrasmall gadolinium oxide (Gd_2O_3) nanoparticles on the surface coating ligand-size was investigated. Both r_1 and r_2 values decreased with increasing ligand-size. We attributed this to the ligand-size effect. In addition the effectiveness of D-glucuronic acid-coated ultrasmall Gd_2O_3 nanoparticles as a T_1 magnetic resonance imaging (MRI) contrast agent was confirmed by measuring the in vitro cytotoxicity and in vivo T_1 MR images in a mouse in a 1.5 T MR field.

Introduction

Nanoparticles are widely used in biomedical applications because of their advanced imaging properties compared to small molecules.[1-4] Surface coating ligands are very important for biomedical applications because most nanoparticles are hydrophobic and toxic.[5,6] Therefore, nanoparticles should be completely coated with hydrophilic and bio-compatible ligands. However, imaging properties of nanoparticles may be affected by the surface coating ligand and thus the ligand effect on imaging properties should be well-documented.

This study focuses on the ligand-size dependent longitudinal (r_1) and transverse (r_2) water proton relaxivities of ultrasmall gadolinium oxide (Gd_2O_3) nanoparticles which are known potential T_1 magnetic resonance imaging (MRI) contrast agents.[7-9] Water-solubility generally increases with increasing ligand-size in the case of hydrophilic ligand,[10] but the ligand-size effect on the r_1 and r_2 values of ultrasmall Gd_2O_3 nanoparticles is unknown. This aspect is thus explored in this study. This information is very important because the MR image quality depends on r_1 and r_2 values. That is, r_1 should be large for T_1 MRI contrast agents, whereas r_2 should be large for T_2 MRI contrast agents. In addition r_2/r_1 ratio should be close to one for T_1 MRI contrast agents.[8,9]

The r_1 and r_2 values depend on various factors such as nanoparticle species, nanoparticle magnetism, particle diameter, hydrodynamic diameter, ligand, solution, pH, temperature, and applied MR field.[11-16] In this study all of the samples were prepared using the same factors except for the ligand. The magnetic properties of lanthanide oxide nanoparticles are not significantly affected by chemical bonding with the ligands because 4f-orbitals of the lanthanides are compact and close to the nucleus.[8,17] Therefore, the r_1 and r_2 values of lanthanide oxide nanoparticles are not significantly affected by chemical bonding with the ligands. This implies that the r_1 and r_2 values of lanthanide oxide nanoparticles is mainly affected by the physical properties of the ligand. Among them, the ligand-size is important because r_1 and r_2 values are proportional to the strength of magnetic dipole interactions between the nanoparticles and surrounding water protons,[12,13,18] and this interaction strength decreases with increasing ligand layer thickness on the nanoparticle surface, which may depend on ligand-size. This corresponds to the ligand-size effect.

This study addressed for the first time the ligand-size dependent r_1 and r_2 values of ultrasmall Gd_2O_3 nanoparticles. The ligands used in this study include D-glucuronic acid, polyethylene glycol diacid (PEGD)-250, and PEGD-600 in the order of increasing ligand-size. All of these ligands are bio-compatible and water-soluble. In addition in vitro cytotoxicity and in vivo T_1 MR images were acquired to confirm the potential of ultrasmall Gd_2O_3 nanoparticles as a T_1 MRI contrast agent.

Experimental

Chemicals

All chemicals including $GdCl_3 \cdot xH_2O$ (99.9%), NaOH (> 99.9%), triethylene glycol (99%), D-glucuronic acid (> 98%), polyethylene glycol diacid (PEGD)-250 (> 96%), and PEGD-600 (> 96%) were purchased from Sigma-Aldrich and used as received. Triply distilled water was used for washing nanoparticle products and preparing aqueous sample solutions.

Synthesis of ligand coated ultrasmall gadolinium oxide (Gd_2O_3) nanoparticles

A reaction scheme for the one-pot synthesis of the ligand coated ultrasmall Gd_2O_3 nanoparticles is shown in Fig. 1. One mmol of $GdCl_3 \cdot xH_2O$ and 3 mmol of ligand (i.e. D-glucuronic

Table 1 Physical data of the three ligands used for surface coating

Ligand	Molecular formula	Molecular mass (amu)	Structure
D-glucuronic acid	$C_{10}H_{10}O_7$	194.14	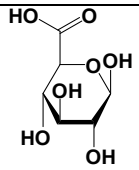
PEGD-250	$HOOCCH_2(OCH_2CH_2)_nOCH_2COOH$ ($n \approx 3$)	250	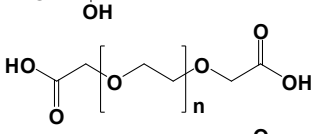
PEGD-600	$HOOCCH_2(OCH_2CH_2)_nOCH_2COOH$ ($n \approx 11$)	600	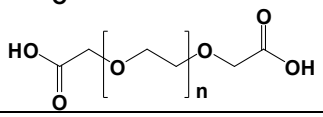

acid or PEGD-250 or PEGD-600) (see Table 1 for ligands) were dissolved in 30 mL of triethylene glycol in a 100 mL three necked flask. The mixture solution was magnetically stirred at ~ 110 °C until the mixture was completely dissolved in triethylene glycol under atmospheric conditions. The NaOH solution was prepared in another beaker by dissolving 3 mmol of NaOH in 5 mL of triethylene glycol, and was then added to the above mixture solution. Then, magnetic stirring was continued at the same temperature for 6 hours. The reaction solution became cloudy because of the formation of ligand coated ultrasmall Gd_2O_3 nanoparticles. The product solution was diluted with 500 mL of triply distilled water. After a week, the nanoparticle products settled to the bottom of the beaker, and the top transparent solution was decanted. During this process, unreacted precursors, free ligand, and solvent were removed. In this way, all three samples were washed for three times. A half volume of each washed sample was diluted with triply distilled water to prepare an aqueous sample solution for MRI experiment, and the remaining half volume was dried in air to powder form for various characterizations.

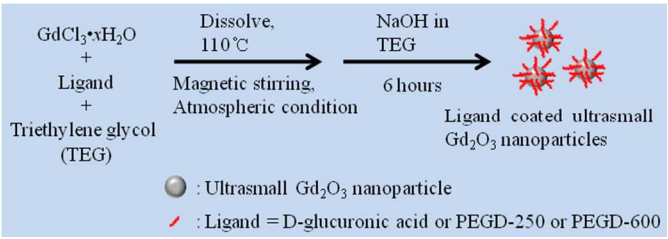

Fig. 1 A scheme for the one-pot synthesis of ligand coated ultrasmall Gd_2O_3 nanoparticles.

Measurements of particle diameter (d), hydrodynamic diameter (a), and crystal structure

A high resolution transmission electron microscope (HRTEM) (FEI, Titan G2 ChemiSTEM CS Probe) operating at 200 kV was used to measure the particle diameter (d) and morphology of the ligand-coated nanoparticles. A drop of each sample solution dispersed in ethanol was placed on a carbon film supported by a 200 mesh copper grid using a micropipette (Eppendorf, 2-20 μL), and allowed to dry in air at room temperature. The copper grid with the nanoparticles was then mounted inside the vacuum chamber for imaging.

A dynamic light scattering (DLS) particle size analyzer (UPA-150, Microtrac) was used to measure the hydrodynamic diameter (a) of the ligand coated nanoparticles. To measure this, a sample solution with concentration of ~ 0.1 mM Gd was used.

A multi-purpose X-ray diffractometer (MP-XRD) (Philips, X'PERT PRO MRD) with unfiltered CuKα (λ = 0.154184 nm) radiation was used to evaluate the crystal structure of the nanoparticles. The scanning step in 2θ was 0.033˚, and the scan range in 2θ was 15 - 100˚.

Surface coating analysis

The attachment of the ligand to the nanoparticles was investigated by recording Fourier transform infrared (FT-IR) absorption spectra using a FT-IR absorption spectrometer (Mattson Instruments, Inc., Galaxy 7020A). To record the FT-IR absorption spectra (650 - 4000 cm^{-1}), a pellet of each powder sample in KBr was prepared.

A thermo-gravimetric analyzer (TGA) (TA Instruments, SDT-Q600) was used to estimate the amount of surface coating on the nanoparticles. Each TGA curve was recorded between room temperature and 900 ˚C with air flowing over the powder sample. The average amount of surface coating by ligand on the nanoparticles was estimated from the mass drop in each TGA curve after taking into account the water desorption between room temperature and ~ 105 °C. After TGA analysis, each TGA analyzed powder sample was collected and subjected to XRD analysis for identification.

Measurements of relaxivities and map images

The Gd concentration of each sample solution was determined using an inductively coupled plasma atomic emission spectrometer (ICPAES, Thermo Jarrell Ash Co., IRIS/AP). The T_1 and T_2 relaxation times and R_1 and R_2 map images of each sample solution were measured using a 1.5 T MRI instrument (GE 1.5 T Signa Advantage, GE medical system) equipped with a knee coil (EXTREM). To measure these, each sample solution was diluted with triply distilled water and a series of solutions with different Gd concentrations (i.e. 0.5, 0.25, 0.125, 0.0625, and 0.0 mM Gd) were prepared. Both relaxation times and map images were then measured using these diluted solutions. r_1 and r_2 relaxivities of each sample solution were estimated from the slopes of the $1/T_1$ and $1/T_2$ plots versus Gd concentration, respectively. The measurement parameters for

both relaxation times and map images were as follows: the external MR field (H) = 1.5 tesla, the temperature (T) = 22 °C, the number of acquisitions (NEX) = 1, the field of view (FOV) = 16 cm, the phase FOV = 0.5, the matrix size = 256 × 128, the slice thickness = 5 mm, the pixel spacing = 0.625 mm, the pixel band width = 122.10 hz, the repetition time (TR) = 2000 ms, and the echo time (TE) = 9 ms.

Measurement of in vitro cytotoxicity

The cellular toxicity of ligand-coated ultrasmall Gd_2O_3 nanoparticles was measured using a CellTiter-Glo Luminescent Cell Viability Assay (Promega, WI, USA). In this assay, the intracellular adenosine-triphosphate (ATP) was quantified using a luminometer (Victor 3, Perkin-Elmer). Both human prostate cancer (DU145) and normal mouse hepatocyte (NCTC1469) cell lines were used. Cells were seeded on a 24-well cell culture plate and incubated for 24 hours (5 % CO_2, 37 ˚C). Five test solutions (i.e. 25, 50, 100, 250, and 500 μM Gd) for each sample solution were prepared by diluting each sample solution with a sterile phosphate-buffered saline (PBS) solution. Approximately 2 μL of each test solution was used to treat the cells. The treated cells were then incubated for 48 hours. The viability of each cell was measured and normalized with respect to the control cell that was not treated with the sample solution. The measurement was repeated two times for each test solution to obtain average cell viabilities.

Measurement of in vivo T_1 MR images

Finally, in vivo T_1 MR images of a mouse were measured using the same 1.5 T MRI instrument used for relaxivity measurement. The animal experiment was carried out with the permission and guidance of the Kyungpook National University (KNU) animal committee. An ICR female mouse (ICR = Institute of Cancer Research, USA) with a weight of ~ 40 g was used for the T_1 MR image measurement. For imaging, the mouse was anesthetized by 1.5% isoflurane in oxygen. Measurements were performed before and after the injection of a sample solution into the mouse tail vein. The injection dose was typically ~ 0.1 mmol Gd/kg. After the measurement, the mouse was revived from anaesthesia and placed in a cage with free access to both food and water. During the measurement, the temperature of each mouse was maintained at ~ 37 ˚C using a warm water blanket. The measurement parameters for T_1 MR images were as follows: the H = 1.5 tesla, the T = 37 ˚C, the NEX = 3, the FOV = 100 mm, the phase FOV = 0.5, the matrix size = 320 x 290, the slice thickness = 1 mm, the spacing gap = 0.5 mm, the pixel bandwidth = 15.63 hz, the TR = 11 ms, and the TE = 3.2 ms.

Results and discussion

Particle diameter (d), hydrodynamic diameter (a), and crystal structure

The HRTEM images of the three samples are shown in Figs. 2a(I)-(III). As shown in Figs. 2a(I)-(III), the ligand coated ultrasmall Gd_2O_3 nanoparticles had nearly monodisperse particle diameters and the average particle diameter (d_{avg}) was estimated to be 1.3 nm for all three samples (Table 2). Nanoparticles were so ultrasmall that it was very difficult to identify them from their lattice images. To solve this, one suspected region as an ultrasmall Gd_2O_3 nanoparticle in each HRTEM image (indicated with a dotted square) in Figs. 2a(I) and (II) was subjected to Fast Fourier Transform (FFT) to obtain a simulated diffraction pattern. Using only the points in each simulated diffraction pattern that were thought to be from the ultrasmall Gd_2O_3 nanoparticle, a simulated lattice image was obtained through inverse Fast Fourier Transform (IFFT). As shown in Figs. 2a(I) and (II), the estimated lattice distance of 3.2 Å in each simulated lattice image was consistent with that (lattice distance L_{222} = 3.121 Å) of cubic Gd_2O_3,[19] confirming that each suspected region corresponds to an ultrasmall Gd_2O_3 nanoparticle. This implies that the dark contrast regions (most likely due to surface coated ligand) with diameters of 1 to 2 nm in HRTEM images correspond to the ligand-coated ultrasmall Gd_2O_3 nanoparticles.

DLS patterns are shown in Fig. 2b. From the log-normal function fit to the observed DLS pattern, the average hydrodynamic diameter (a_{avg}) was estimated to be 6.2 nm for D-glucuronic acid coated ultrasmall Gd_2O_3 nanoparticles, 9.7 nm for PEGD-250 coated ultrasmall Gd_2O_3 nanoparticles, and 12.1 nm for PEGD-600 coated ultrasmall Gd_2O_3 nanoparticles (Table 2). This increase in hydrodynamic diameter with increasing ligand-size showed that the ligand layer thickness on the nanoparticle surface increased with increasing ligand-size.

The XRD patterns of the three powder samples were broad and amorphous as shown in Fig. 3. This is likely due to the ultrasmall particle diameters.[20] However, sharp peaks were observed after the TGA analyses of the three samples, corresponding to a cubic structure of bulk Gd_2O_3 as shown in Fig. 3. This is due to the crystal growth upon heat treatment up to 900 ºC, as previously observed.[21] The estimated cell constant of all three TGA analyzed samples was 10.815 Å, which is consistent with the reported value of 10.813 Å.[19]

Ligand surface coating analysis

The three ligands used for surface coating are provided in Table 1. They are D-glucuronic acid, PEGD-250, and PEGD-600. Surface coating of the three samples was investigated by recording the FT-IR absorption spectra as shown in Fig. 4. The characteristic IR stretches of the C-H at 2850 - 2940 cm^{-1}, the C=O at 1580 - 1650 cm^{-1}, and the C-O at 1060 - 1110 cm^{-1} showed the presence of the corresponding ligand in the nanoparticles. The red-shift of the C=O stretch by 90 - 150 cm^{-1} from those of the corresponding free acids (labeled as C=O* in Fig. 4 and occurring at 1710 - 1740 cm^{-1}) showed that the -COOH group was chemically bonded to the nanoparticle. This red-shift had been observed in various metal oxide nanoparticles coated by various ligands with -COOH groups,[20,22-25] supporting our results. In the case of the PEGD-600 coated nanoparticles, the free C=O* stretch was not observed, implying that both of the -COOH groups in PEGD-600 were bonded to the nanoparticle. This is likely because PEGD-600 has a long and flexible chain length. On the other hand, both the free C=O* and bonded C=O stretches with almost equal intensities were observed in the PEGD-250 coated ultrasmall Gd_2O_3 nanoparticles, implying that only one of the two -COOH groups in PEGD-250 was bonded to the nanoparticle. This is likely because PEGD-250 has a short chain length. As a result, absorption intensities of the free C=O* and bonded C=O stretches in the PEGD-250 coated ultrasmall Gd_2O_3 nanoparticles were much weaker than those of the bonded C=O stretches in the D-glucuronic acid and PEGD-600 coated ultrasmall Gd_2O_3 nanoparticles.

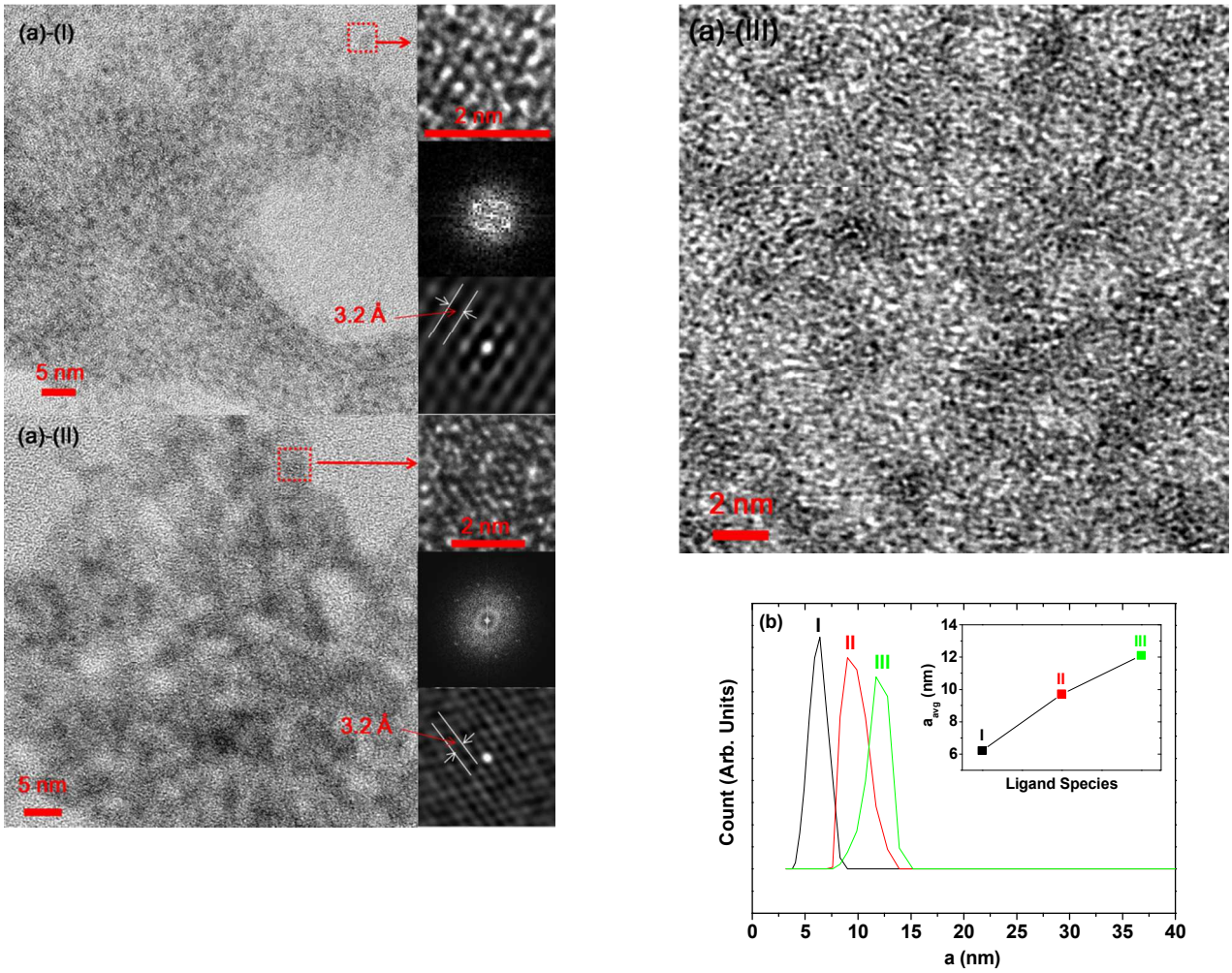

Fig. 2 (a) HRTEM images and (b) hydrodynamic diameters: (I) D-glucuronic acid, (II) PEGD-250, and (III) PEGD-600 coated ultrasmall Gd_2O_3 nanoparticles. For both (I) and (II), a simulated diffraction pattern and simulated lattice image are provided to confirm that each suspected region in the HRTEM image (indicated with a dotted square) corresponds to an ultrasmall Gd_2O_3 nanoparticle. Inset in (b) is a plot of the a_{avg} as a function of ligand species (i.e. ligand-size).

Table 2 Average particle diameter (d_{avg}), average hydrodynamic diameter (a_{avg}), surface coating property, and water proton relaxivity

Ligand	d_{avg} (nm)	a_{avg} (nm)	Surface coating property			Relaxivity ($s^{-1}mM^{-1}$)	
			P (%)[a]	σ ($1/nm^2$)[b]	N[c]	r_1	r_2
D-glucuronic acid	1.3	6.2	53	8	42	24 ± 2	60 ± 5
PEGD-250	1.3	9.7	39	3	16	5 ± 1	55 ± 2
PEGD-600	1.3	12.1	40	1	6	0.1 ± 0.1	10 ± 1

[a]Average ligand surface coating amount in weight percent estimated from the TGA curve.
[b]Grafting density = average number of ligands coated per unit surface area of a nanoparticle.
[c]Average number of ligands coated per nanoparticle = $\sigma \times \pi d_{avg}^2$.

A sufficient surface coating is crucial for biomedical applications. The average amount (P) of ligand coated on the nanoparticle surface in weight percent (%) was estimated from the mass drop in each TGA curve as shown in Fig. 5, and the results are provided in Table 2. Here, the water desorption between room temperature and ~ 105 °C was taken into account as shown in Fig. 5. As given in Table 2, all of the three samples were sufficiently coated with the corresponding ligand. The grafting density (σ) corresponding to the average number of ligands coated per unit surface area of a nanoparticle[26] was estimated using the bulk density of Gd_2O_3 (= 7.407 g/cm^3),[27] surface coating weight percent estimated from the corresponding TGA curve, and average particle diameter estimated from the corresponding HRTEM image. As provided in Table 2, the estimated σ values in all three samples were larger than 1.0 nm^{-2}, confirming that all three samples were sufficiently coated with the corresponding ligand.[26] The remaining mass in each TGA curve corresponds to the average net mass of the nanoparticles in ligand coated nanoparticles. By multiplying the estimated σ by the nanoparticle surface area (= πd_{avg}^2), the average number (N) of ligands coated per nanoparticle was estimated. As given in Table 2, the N value

decreased with increasing ligand-size. This is likely because a larger ligand can show a larger steric hindrance to surface coating and consequently fewer ligands coat on the nanoparticle surface.

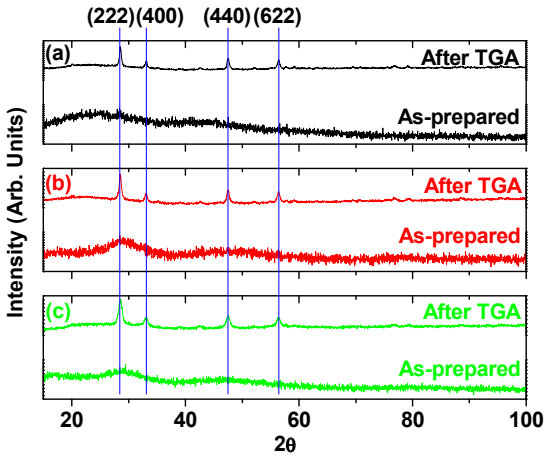

Fig. 3 Powder XRD patterns of as-synthesized and TGA-treated (a) D-glucuronic acid, (b) PEGD-250, and (c) PEGD-600 coated ultrasmall Gd_2O_3 nanoparticles. XRD patterns of TGA treated powder samples are assigned with Miller index (hkl).

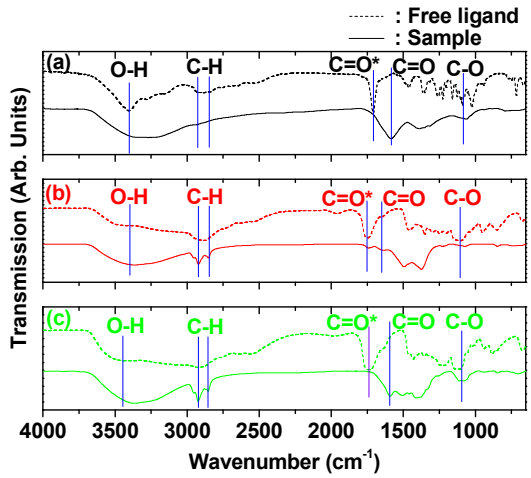

Fig. 4 FT-IR absorption spectra of powder samples of (a) D-glucuronic acid, (b) PEGD-250, and (c) PEGD-600 coated ultrasmall Gd_2O_3 nanoparticles and respective free ligands. Stretches of O-H, C-H, free C=O*, bonded C=O, and C-O are assigned in each spectrum.

Ligand surface coating structure

Based on the observed FT-IR absorption spectra, the most probable ligand surface coating structures of the three samples are schematically drawn in Figs. 6a-c. As discussed before, the –COOH group of the ligand is bonded to the Gd^{3+} on the nanoparticle surface. A half molecular length of PEGD-600 (i.e. n/2 ≈ 5.5, n = polymer repeating unit) in Fig. 6c is still longer than the full molecular length of PEGD-250 (n ≈ 3) in Fig. 6b. This will explain the larger hydrodynamic diameter of the PEGD-600 coated ultrasmall Gd_2O_3 nanoparticles compared to PEGD-250 coated ultrasmall Gd_2O_3 nanoparticles.

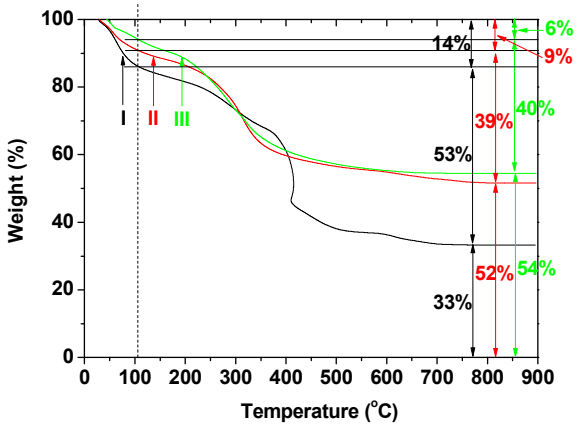

Fig. 5 TGA curves of powder samples of (I) D-glucuronic acid, (II) PEGD-250, and (III) PEGD-600 coated ultrasmall Gd_2O_3 nanoparticles.

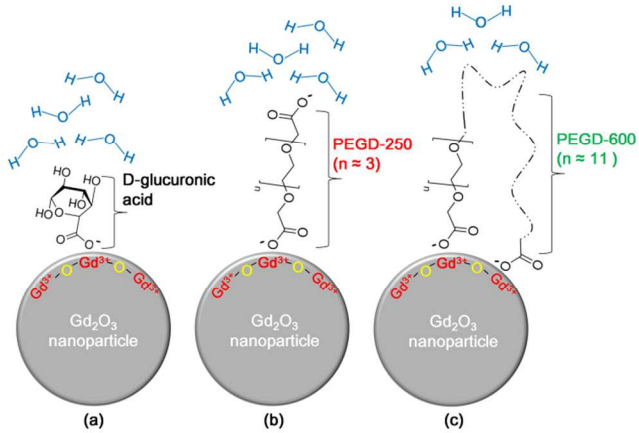

Fig. 6 The most probable surface coating structures of (a) D-glucuronic acid, (b) PEGD-250, and (c) PEGD-600 on the ultrasmall Gd_2O_3 nanoparticle surface, based on FT-IR absorption spectra.

Ligand-size dependent water proton relaxivities: the ligand-size effect

As shown in Fig. 7a, r_1 and r_2 values of the three samples were estimated from the slopes of the plots of $1/T_1$ and $1/T_2$ inverse water proton relaxation times as a function of Gd concentration, respectively (Table 2). They are also plotted as a function of ligand species (i.e. ligand-size) in Fig. 7b, showing that both r_1 and r_2 values decreased with increasing ligand-size. As shown in Fig. 7c, R_1 and R_2 map images also clearly showed the contrast enhancements in all three samples (0.5 mM Gd) with respect to the control (0.0 mM Gd), but the contrast enhancements were reduced with increasing ligand-size because the relaxivities decreased accordingly.

As mentioned before, the ligand layer thickness increased with increasing ligand-size, which was confirmed from the hydrodynamic diameters (see Fig. 2b). Therefore, less water will access the Gd_2O_3 nanoparticle. This imples that r_1 and r_2 values will decrease with increasing ligand-size (i.e., the ligand-size effect). This explains the observed ligand-size

dependent r_1 and r_2 values. However, further investigations will be needed for a full understanding for this.

It is worth mentioning that a large r_1 value, water-solubility, biocompatibility, and renal excretion are crucial for in vivo applications of ligand coated ultrasmall Gd_2O_3 nanoparticles as a T_1 MRI contrast agent. For water-solubility and biocompatibility a large ligand is generally better.[28] However, for a large r_1 value and renal excretion[29] a small ligand is better. This opposite result may be unraveled using highly water-soluble small ligand coatings. One example includes a small zwitterionic coating on a quantum dot such as the amino acid cysteine which showed a high water-solubility and a small hydrodynamic diameter.[29]

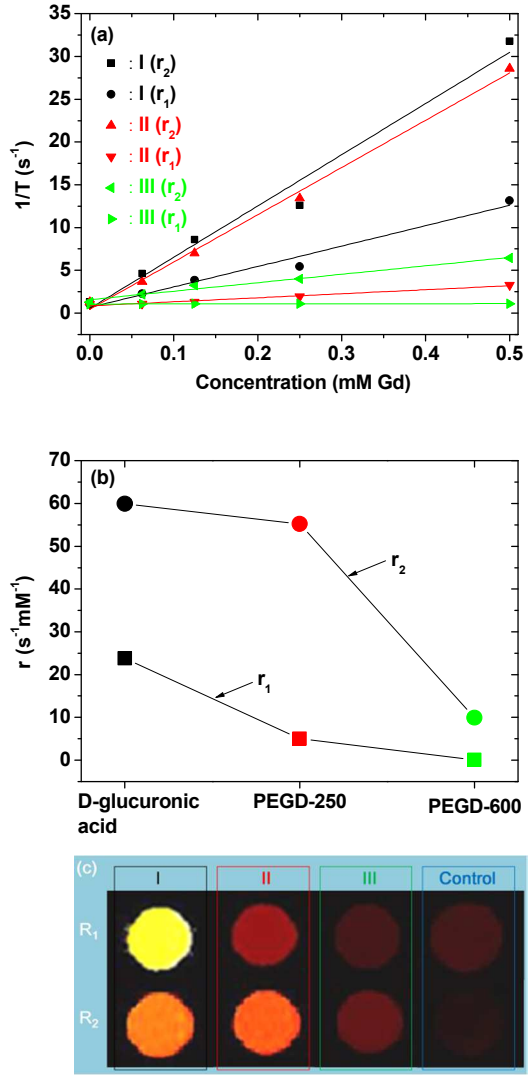

Fig. 7 (a) Plots of $1/T_1$ and $1/T_2$ as a function of Gd concentration, (b) plots of r_1 and r_2 values as a function of ligand species (i.e. ligand-size), and (c) R_1 and R_2 map images at 0.0 (i.e. control) and 0.5 mM Gd concentrations of sample solutions: (I) D-glucuronic acid, (II) PEGD-250, and (III) PEGD-600 coated ultrasmall Gd_2O_3 nanoparticles.

Reduced r_1 and r_2 values in Gd_2O_3-OA-CTAB nanoparticles (OA = oleic acid and CTAB = cetyltrimethylammonium bromide) were observed, compared to Gd_2O_3-PVP nanoparticles (PVP = polyvinyl pyrrolidone).[30] This was explained in such a way that the bi-layer long hydrophobic chains in OA-CTAB effectively prevented the water molecules from approaching the Gd_2O_3 nanoparticles, whereas the polar C=O group in each monomer of PVP allowed the water molecules to pass through the PVP coating layer, and thus to interact with Gd_2O_3. This situation is very similar to the present ligand-size dependent case, supporting our results. That is, smaller ligands will allow more water molecules to access the core Gd_2O_3 nanoparticles than large ligands can do. As mentioned in the Introduction section, r_1 and r_2 values depend on many factors. As an example, Engström et al. observed that r_1 and r_2 values of Gd_2O_3 nanoparticles somewhat depended on solution.[31] Ahrén et al. observed that surface modification enhanced not only the stability and biocompatibility, but also the relaxivity of Gd_2O_3 nanoparticles.[32] All of these works including the present work suggest that r_1 and r_2 values depend on many factors, and among them the ligand plays an important role in r_1 and r_2 values.

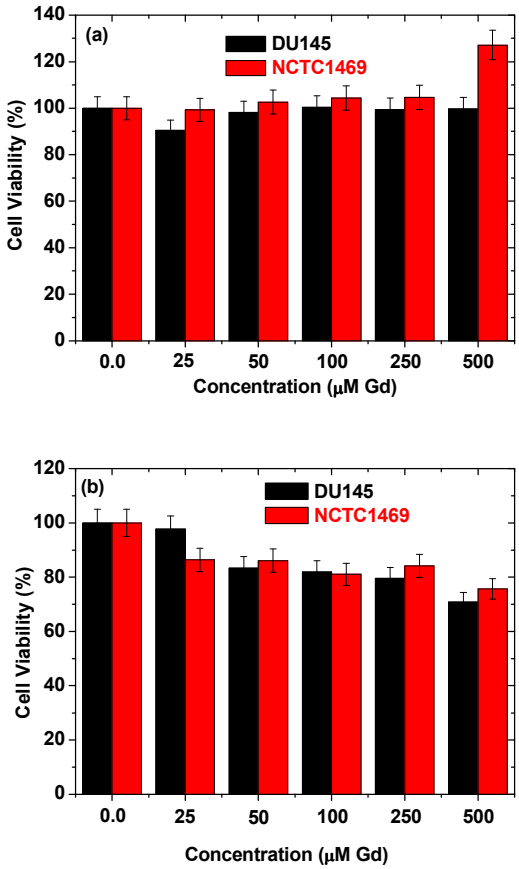

Fig. 8 In vitro cytotoxicity of sample solutions of (a) D-glucuronic acid coated and (b) PEGD-250 coated ultrasmall Gd_2O_3 nanoparticles using DU145 and NCTC1469 cell lines, showing non-toxicity up to 500 μM Gd.

In vivo T_1 MR images in a 1.5 T MR field

Before in vivo applications, biocompatibility of the synthesized nanoparticles was proved from in vitro cytotoxicity test using both DU145 and NCTC1469 cell lines. Of the three samples, sample solutions of D-glucuronic acid coated and PEGD-250 coated ultrasmall Gd_2O_3 nanoparticles were subjected to the test. As shown in Fig. 8, both samples were non-toxic for the

Gd-concentration range up to 500 μM in both cell lines. This level of cytotoxicity was sufficient for an in vivo MRI experiment. In vivo T_1 MR images were obtained using a sample solution of D-glucuronic acid coated ultrasmall Gd_2O_3 nanoparticles because it has the largest r_1 value. The sample solution was injected into a mouse tail vein and a series of 1.5 T T_1 MR images were obtained as a function of time. The results are provided in Fig. 9. Positive (i.e. brighter) contrast enhancements in both the liver and kidneys were observed in both the axial and coronal T_1 MR images. These results confirm that the D-glucuronic acid coated ultrasmall gadolinium oxide nanoparticles are a potential T_1 MRI contrast agent.

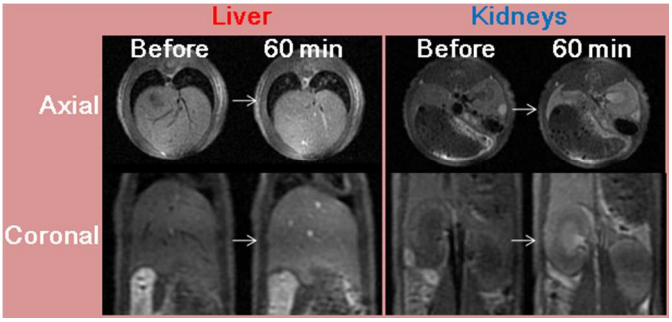

Fig. 9 In vivo axial and coronal T_1 MR images of kidneys and liver in a mouse in a 1.5 T MR field before and 60 minutes after intravenous injection of a sample solution of D-glucuronic acid coated ultrasmall Gd_2O_3 nanoparticles into a mouse tail.

Conclusions

In summary we addressed for the first time the ligand-size dependent r_1 and r_2 water proton relaxivities of ultrasmall Gd_2O_3 nanoparticles. The three ligands used include D-glucuronic acid, PEGD-250, and PEGD-600 in order of increasing ligand-size. The results are summarized as follows.

(1) Both r_1 and r_2 values decreased with increasing ligand-size.

(2) The observed ligand-size dependent r_1 and r_2 values were qualitatively explained using the ligand-size effect. That is, r_1 and r_2 values decreased with increasing ligand-size. Further investigations will be needed for a full understanding for this.

(3) Finally the potential of the ultrasmall Gd_2O_3 nanoparticles as a T_1 MRI contrast agent was proved by measuring in vitro cytotoxicity and in vivo T_1 MR images in a 1.5 T MR field: sample solutions were non-toxic and clear positive contrast enhancements were observed in the liver and kidneys in a mouse after intravenous injection of a sample solution.

Acknowledgments

This study was supported by the Basic Science Research Program (Grant No. 2014-005837 to YC and 2013R1A1A4A03004511 to GHL) and the Basic Research Laboratory (BRL) Program (Grant No. 2013R1A4A1069507) of the National Research Foundation funded by the Ministry of Education, Science, and Technology. This study was also supported by the R&D program of MKE/KEIT (Grant No. 10040393, development and commercialization of molecular diagnostic technologies for lung cancer through clinical validation). The authors wish to thank the Korea Basic Science Institute for the use of their HRTEM and XRD.

Notes and references

[a] Department of Chemistry, College of Natural Sciences, Kyungpook National University (KNU), Taegu 702-701, South Korea. Email: ghlee@mail.knu.ac.kr. Tel: -82-53-950-5340. Fax: -82-53-950-6330.
[b] Department of Molecular Medicine and Medical & Biological Engineering, School of Medicine, KNU and Hospital, Taegu 702-701, South Korea. Email: ychang@knu.ac.kr.
[c] Department of Nanoscience and Nanotechnology, KNU, Taegu 702-701, South Korea.
[d] Department of Biology Education, Teachers' College, KNU, Taegu 702-701, South Korea.

See DOI: 10.1039/b000000x/

1 Q. A. Pankhurst, N. K. T. Thanh, S. K. Jones and J. Dobson, Progress in applications of magnetic nanoparticles in biomedicine, *J. Phys. D: Appl. Phys*., 2009, **42**, 224001 (15 pages).

2 A. G. Roca, R. Costo, A. F. Rebolledo, S. Veintemillas-Verdaguer, P. Tartaj, T. González-Carreño, M. P. Morales and C. J. Serna, Progress in the preparation of magnetic nanoparticles for applications in biomedicine, *J. Phys. D: Appl. Phys*., 2009, **42**, 224002 (11 pages).

3 C. C. Berry, Progress in functionalization of magnetic nanoparticles for applications in biomedicine, *J. Phys. D: Appl. Phys*., 2009, **42**, 224003 (9 pages).

4 O. V. Salata, Applications of nanoparticles in biology and medicine, *J. Nanobiotechnology*, 2004, **2**: 3 (6 pages).

5 R. Hardman, A toxicologic review of quantum dots: toxicity depends on physicochemical and environmental factors, *Environ. Health Perpect.*, 2006, **114**, 165-172.

6 A. Nel, T. Xia and N. Li, Toxic potential of materials at the nanolevel, *Science*, 2006, **311**, 622-627.

7 G. H. Lee, Y. Chang and T. J. Kim, Blood-pool and targeting MRI contrast agents: from Gd-chelates to Gd-nanoparticles, *Eur. J. Inorg. Chem*., 2012, 1924-1933.

8 W. Xu, K. Kattel, J. Y. Park, Y. Chang, T. J. Kim and G. H. Lee, Paramagnetic nanoparticle T_1 and T_2 MRI contrast agents, *Phys. Chem. Chem. Phys*., 2012, **14**, 12687-12700.

9 T. J. Kim, K. S. Chae, Y. Chang and G. H. Lee, Gadolinium oxide nanoparticles as potential multimodal imaging and therapeutic agents, *Curr. Top. Med. Chem*., 2013, **13**, 422-433.

10 J. S. Bradley, in Clusters and Colloids, ed. G. Schmid, Weinheim, VCH, 1994, pp. 465-469.

11 J. Y. Park, M. J. Baek, E. S. Choi, S. Woo, J. H. Kim, T. J. Kim, J. C. Jung, K. S. Chae, Y. Chang and G. H. Lee, Paramagnetic ultrasmall gadolinium oxide nanoparticles as advanced T_1 MRI contrast agent: account for large longitudinal relaxivity, optimal particle diameter, and in vivo T_1 MR images, *ACS Nano*, 2009, **3**, 3663-3669.

12 R. B. Lauffer, Paramagnetic metal complexes as water proton relaxation agents for NMR imaging: theory and design, *Chem. Rev*., 1987, **87**, 901-927.

13 A. Roch, R. N. Muller and P. Gillis, Theory of proton relaxation induced by superparamagnetic particles, *J. Chem. Phys*., 1999, **110**, 5403-5411.

14 Y. Gossuin, A. Hocq, Q. L. Vuong, S. Disch, R. P. Hermann and P. Gillis, Physico-chemical and NMR relaxometric characterization of gadolinium hydroxide and dysprosium oxide nanoparticles, *Nanotechnology*, 2008, **19**, 475102 (8 pages).

15 M. Norek, E. Kampert, U. Zeitler and J. A. Peters, Tuning of the size of Dy_2O_3 nanoparticles for optimal performance as an MRI contrast agent, *J. Am. Chem. Soc*., 2008, **130**, 5335-5340.
16 M. Norek, G. A. Pereira, C. F. G. C. Geraldes, A. Denkova, W. Zhou and J. A. Peters, NMR transversal relaxivity of suspensions of lanthanide oxide nanoparticles, *J. Phys. Chem. C*, 2007, **111**, 10240-10246.
17 F. A. Cotton and G. Wilkinson, Advanced Inorganic Chemistry, A Wiley-Interscience Publication, New York, 4th edn., 1980, pp. 984.
18 B. D. Cullity, Introduction to Magnetic Materials, Addison-Wesley Publishing Company, Reading, 1972, pp. 616.
19 JCPDS-International Centre for Diffraction Data, card no. 43-1014, PCPDFWIN, vol. 1.30, 1997.
20 F. Söderlind, H. Pedersen, R. M. Petoral Jr., P. -O. Käll and K. Uvdal, Synthesis and characterization of Gd_2O_3 nanocrystals functionalized by organic acids, *J. Colloid Interface Sci.*, 2005, **288**, 140-148.
21 K. Kattel, J. Y. Park, W. Xu, H. G. Kim, E. J. Lee, B. A. Bony, W. C. Heo, J. J. Lee, S. Jin, J. S. Baeck, Y. Chang, T. J. Kim, J. E. Bae, K. S. Chae and G. H. Lee, A facile synthesis, in vitro and in vivo MR studies of D-glucuronic acid-coated ultrasmall Ln_2O_3 (Ln = Eu, Gd, Dy, Ho, and Er) nanoparticles as a new potential MRI contrast agent, *ACS Appl. Mater. Interfaces*, 2011, **3**, 3325-3334.
22 O. W. Duckworth and S. T. Martin, Surface complexation and dissolution of hematite by C_1-C_6 dicarboxylic acids at pH = 5.0, *Geochim. Cosmochim. Acta*, 2001, **65**, 4289-4301.
23 S. J. Hug and D. Bahnemann, Infrared spectra of oxalate, malonate and succinate adsorbed on the aqueous surface of rutile, anatase and lepidocrocite measured with in situ ATR-FTIR, *J. Electron Spectro. Related Phenomena*, 2006, **150**, 208-219.
24 S. J. Hug and B. Sulzberger, In situ fourier transform infrared spectroscopic evidence for the formation of several different surface complexes of oxalate on TiO_2 in the aqueous phase, *Langmuir*, 1994, **10**, 3587-3597.
25 C. B. Mendive, T. Bredow, M. A. Blesa and D. W. Bahnemann, ATR-FTIR measurements and quantum chemical calculations concerning the adsorption and photoreaction of oxalic acid on TiO_2, *Phys. Chem. Chem. Phys.*, 2006, **8**, 3232-3247.
26 M. K. Corbierre, N. S. Cameron and R. B. Lennox, Polymer-stabilized gold nanoparticles with high grafting densities, *Langmuir*, 2004, **20**, 2867-2873.
27 Aldrich Catalog, 2005-2006, pp. 1260.
28 H. T. Uyeda, I. L. Medintz, J. K. Jaiswal, S. M. Simon and H. Mattoussi, Synthesis of compact multidentate ligands to prepare stable hydrophilic quantum dot fluorophores, *J. Am. Chem. Soc*., 2005, **127**, 3870-3878.
29 H. S. Choi, W. Liu, P. Misra, E. Tanaka, J. P. Zimmer, B. I. Ipe, M. G. Bawendi and J. V. Frangioni, Renal clearance of quantum dots, *Nat. Biotechnology*, 2007, **25**, 1165-1170.
30 J. Fang, P. Chandrasekharan, X.-L. Liu, Y. Yang, Y.-B. Lv, C.-T. Yang and J. Ding, Manipulating the surface coating of ultra-small Gd_2O_3 nanoparticles for improved T_1-weighted MR imaging, *Biomaterials*, 2014, **35**, 1636-1642.
31 M. Engström, A. Klasson, H. Pedersen, C. Vahlberg, P.-O. Käll and K. Uvdal, High proton relaxivity for gadolinium oxide nanoparticles, *Magn. Reson. Mater. Phy*., 2006, **19**, 180-186.
32 M. Ahrén, L. Selegård, A. Klasson, F. Söderlind, N. Abrikossova, C. Skoglund, T. Bengtsson, M. Engström, P.-O. Käll and K. Uvdal, Synthesis and characterization of PEGylated Gd_2O_3 nanoparticles for MRI contrast enhancement, *Langmuir*, 2010, **26**, 5753-5762.

